OXFORD

SOT | Society of Toxicology
academic.oup.com/toxsci

Tox Spotlight article

TOXICOLOGICAL SCIENCES, 172(2), 2019, 411–416

doi: 10.1093/toxsci/kfz183
Advance Access Publication Date: August 14, 2019
Research Article

Titanium Dioxide Nanoparticles Elicit Lower Direct Inhibitory Effect on Human Gut Microbiota Than Silver Nanoparticles

Richard T. Agans,*,[1] Alex Gordon,*,[1] Saber Hussain,† and Oleg Paliy*,[2]

*Department of Biochemistry and Molecular Biology, Boonshoft School of Medicine, Wright State University, Dayton, Ohio; and †Molecular Mechanisms Branch, Bioeffects Division, Airman Systems Directorate, 711 Human Performance Wing, Wright-Patterson Air Force Base, Dayton, Ohio

[1]These authors contributed equally to this study.
[2]To whom correspondence should be addressed at Department of Biochemistry and Molecular Biology, Boonshoft School of Medicine, 260 Diggs Laboratory, Wright State University, 3640 Col. Glenn Hwy, Dayton, OH 45435. Fax: 937-775-3730; E-mail: oleg.paliy@wright.edu

ABSTRACT

Due to continued technological development, people increasingly come in contact with engineered nanomaterials (ENMs) that are now used in foods and many industrial applications. Many ENMs have historically been shown to possess antimicrobial properties, which has sparked concern for how dietary nanomaterials impact gastrointestinal health via microbial dysbiosis. We employed an *in vitro* Human Gut Simulator system to examine interactions of dietary nano titanium dioxide (TiO_2) with human gut microbiota. Electron microscopy indicated a close association of TiO_2 particles with bacterial cells. Addition of TiO_2 to microbial communities led to a modest reduction in community density but had no impact on community diversity and evenness. In contrast, administration of known antimicrobial silver nanoparticles (NPs) in a control experiment resulted in a drastic reduction of population density. In both cases, communities recovered once the addition of nanomaterials was ceased. Constrained ordination analysis of community profiles revealed that simulated colonic region was the primary determinant of microbiota composition. Accordingly, predicted community functional capacity and measured production of short-chain fatty acids were not changed significantly upon microbiota exposure to TiO_2. We conclude that tested TiO_2 NPs have limited direct effect on human gut microbiota.

Key words: microbiota; nanoparticles; titanium oxide; silver.

Engineered nanomaterials (ENMs) continue to see increased use in many applications across military, industrial, and consumer space. The ability to produce new and increasingly complex ENMs continues to surpass the ability to assess biomolecular interactions of ENMs and their potential cytotoxicity. The toxic potential of ENMs is influenced by their unique physicochemical properties, including their size, charge, geometry, surface functionalization, and the formation and composition of protein corona around them (Gunawan *et al.*, 2014; Hu *et al.*, 2016). The combination of these properties may enable increased uptake of ENMs into the body, induction of pro-inflammatory cytokines, increased apoptosis, or a higher rate of cell death (Hu *et al.*, 2016; Wiesenthal *et al.*, 2011).

Exposure to ENMs occurs via respiratory, gastrointestinal, or other epidermal routes (Basinas *et al.*, 2018; Pietroiusti *et al.*, 2017). Mainstream focus for ENM-induced exposure and toxicity has centered on the respiratory route, where acute inhalation of ENMs results in a rapid toxicity (Bakand *et al.*, 2012). Exposure via the gastrointestinal route is less studied. Gastrointestinal exposure to ENMs can occur by the ingestion of dietary products containing ENMs (eg used as colorant, preservative, or filler) or as a secondary exposure from the respiratory clearance of ENMs through the mucociliary escalator (Pietroiusti *et al.*, 2017). Examples of foods with high titanium dioxide (TiO_2) amounts include candies and chewing gums. Among household products, toothpastes and some sunscreens can contain up to 10%

of titanium by weight, and TiO_2 is commonly used in white paints and paper (Weir *et al.*, 2013). Upon entering the body via the gastrointestinal tract, ENMs are acidified in the stomach. This acidification has been shown to increase ENM toxicity via ion shedding (Pietroiusti *et al.*, 2017). Following transfer from the stomach into the small intestine, ENMs begin to encounter a myriad of proteins and peptides. These range in size and charge, and can interact with ENMs by creating coronas around them, causing agglomeration and altering ENM charge (Gunawan *et al.*, 2014). Of the research conducted on gut interactions with ENMs, the majority of studies focused on the direct interactions with gut epithelial cells (Pietroiusti *et al.*, 2017). Little work has been conducted, however, assessing ENM interactions with gut microbiota and downstream impacts on host health.

The gut microbiota is intricately involved in host health through the digestion of dietary fiber and other nutrients, modulation of host immune responses and gut transit, and by fighting pathogenic invaders (Sekirov *et al.*, 2010). The composition of the microbiota can be influenced by many exogenous factors including macronutrient content of the diet, changes in host physiology, invasion and colonization by foreign species, use of antibiotics, and possibly ENMs (Pietroiusti *et al.*, 2017). In a healthy state, the microbiota has a commensal relationship with the host; however, this relationship can be influenced by the factors listed above, creating a state of microbial dysbiosis (Hollister *et al.*, 2014). Such dysbiosis can lead to changes in fermentation end products and mucin layer thickness, production of chemicals that promote inflammation of host tissues and cause increased intestinal permeability, and alterations of bowel habits (Gorkiewicz and Moschen, 2018). Thus, the interactions between gut microbiota and ENMs can impact host health directly, through modification of ENMs by microbiota (increasing toxicity), or indirectly through ENM-induced dysbiosis of gut microbial communities.

Previous studies have highlighted the potential toxicity of different ENMs using various cell and animal models, but the findings have not been consistent among the reports (Pietroiusti *et al.*, 2017). For example, TiO_2 particles elicited a cytotoxic response in colon cell culture models, however, the effect was not reproducible in alternative cultures or animal models (Pietroiusti *et al.*, 2017). Similarly, silver (Ag) nanoparticles (NPs) elicited a toxic effect in monocultures and animals, but this effect was not observed in the *in vitro* co- and tricultures (van den Brule *et al.*, 2016). The lack of consistency could be explained by the differences in various models used. It could also be influenced by the different interactions of microbial cells with ENMs because *in vivo* studies that focused on ENM biomolecular interactions were not able to separate microbiota effects from the direct interactions of ENMs with the host tissues. In order to eliminate possible confounding effects of NPs on the host physiology in turn affecting gut microbes, we utilized a recently established *in vitro* Human Gut Simulator (HGS) to study the impact of TiO_2 and Ag NPs on human gut microbiota (Agans *et al.*, 2018). This *in vitro* system mimics the environmental conditions of the human colon, but does not incorporate host tissues or metabolites, thus allowing us to test direct effects of NPs on microbial populations.

MATERIALS AND METHODS

Experimental design. The design and validation of a three vessel *in vitro* HGS system has been described recently (Agans *et al.*, 2018). Briefly, HGS system consisted of three continuously linked fermentation vessels maintained under anaerobic atmosphere, each mimicking a different region of the colon: vessel 1 simulated proximal colon, vessel 2—transverse colon, and vessel 3—distal colon. The medium which closely matched food bolus contents that reach the colon in subjects consuming typical Western diet (Agans *et al.* 2018) was supplied to vessel 1, and vessel contents were moved "along the colon" in 42 ml pulses every 2 h. The environmental conditions (temperature, pH, relative volume, and contents movement) in each vessel matched those experimentally measured in the corresponding section of the human gut.

Human Gut Simulator was seeded with distal gut microbiota collected from three healthy male volunteers (27–31 years old) with no recent history (6 months) of antibiotic or probiotic use, and no gastrointestinal illness (Agans *et al.*, 2018). Following a 14 day community stabilization period, TiO_2 and Ag NPs were administered at 100 mg/day dose for 7 days followed by a 7 day "rescue" period without NP treatment (see Figure 1A). Nanoparticles were pre-mixed in anaerobic phosphate buffered saline (PBS) buffer and were added to vessel 1 of the HGS system daily via syringe. Two replicate runs with TiO_2 were conducted; a single Ag NPs run was also carried out as control. Cytometric analysis via phase contrast microscopy was performed every 48 h to allow real-time assessment of microbial community density.

Nanoparticle characterization. Titanium dioxide (approximately 25 nm in diameter) and silver (30–50nm) NPs were obtained from Evonik Industries and US Research Nanomaterials, respectively. All NPs were measured for hydrodynamic and surface charge in ultrapure H_2O and in Western medium (omitting carbohydrates for NP diameter measurements) using a Malvern Zetasizer and scanning transmission electron microscopy with Electron Dispersive X-ray (STEM/EDX) as we described previously (West *et al.*, 2016).

Microbial genomic DNA isolation and high throughput sequencing. Isolation of microbial genomic DNA from HGS samples was performed using ZR Fungal/Bacterial DNA Miniprep kit (Zymo Research), as we did previously (Rigsbee *et al.*, 2011). Amplification of gDNA targeted the 16S rRNA gene V4 region using conserved primers (forward sequence GCCAGCMGCCGCGG and reverse GGACTACHVGGGTWTCTAAT complementary sequence). Forward primers contained Ion Torrent P1 adapter sequence and 6–7 nucleotide barcode sequence; reverse primer sequences included adapter A. PCR amplification was performed with 25 ng of starting gDNA material and included 10 cycles of linear elongation with only the forward primer used, followed by 25 cycles of traditional exponential PCR (Paliy and Foy, 2011). Inclusion of linear PCR step decreased the stochasticity of the first few PCR reaction steps and allowed the use of a single PCR amplification reaction per sample. Template preparation and sequencing on Ion Torrent PGM were performed as described (Agans *et al.*, 2018). We obtained an average of 9742 sequences per sample. Sequence reads were processed in QIIME (Caporaso *et al.*, 2010). Annotation of operational taxonomic units was performed via open reference method against Ribosome Database Project reference database of 16S rRNA sequences. Sequence read counts for each operational taxonomic unit (OTU) were adjusted by dividing them by known or predicted number of 16S rRNA gene copies in that organism's genome following a previously described approach (Rigsbee *et al.*, 2011). The adjusted read counts were then converted to a sample-specific cell number based on the previously determined cell density measurements for each sample. As a result,

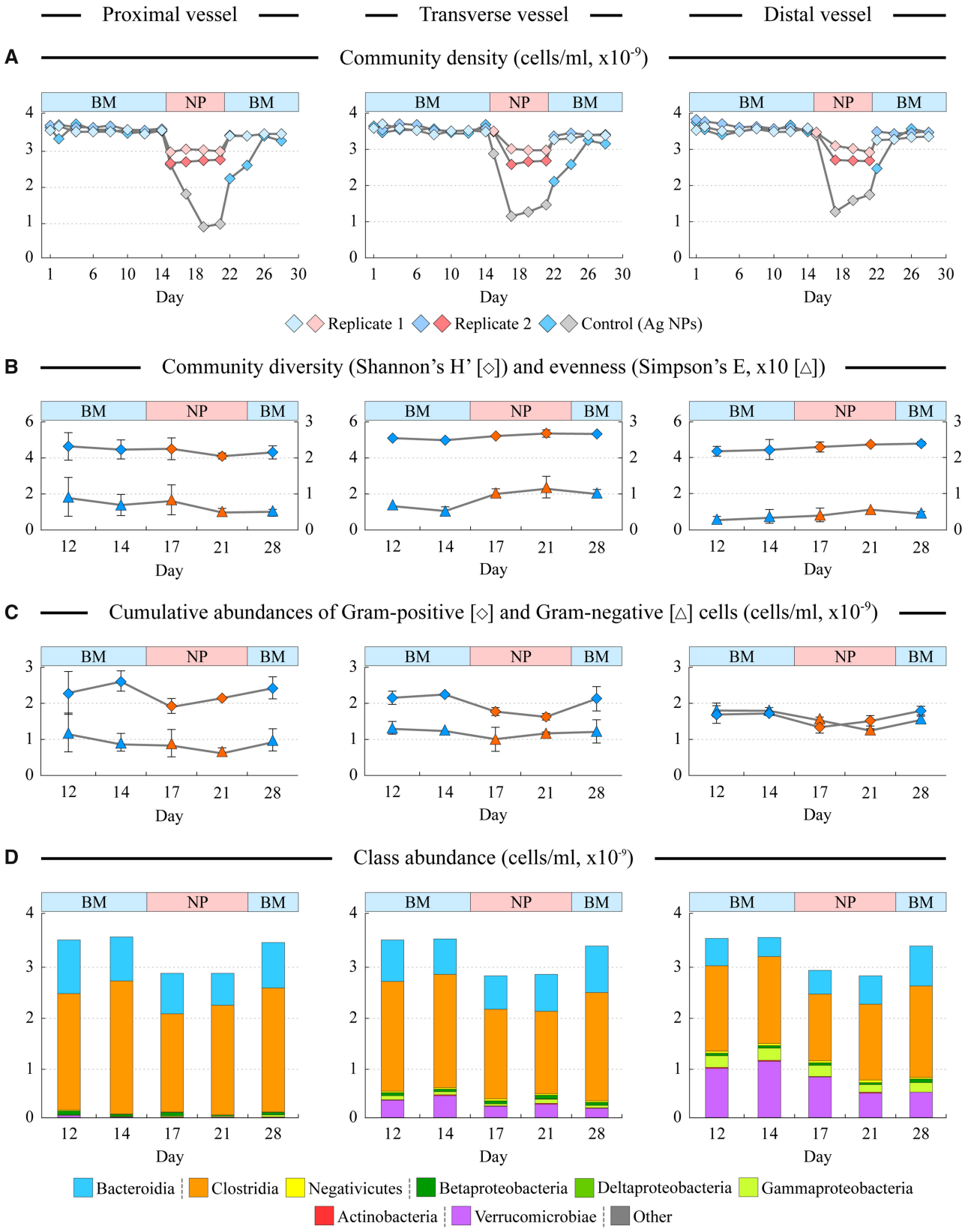

Figure 1. Changes in microbial community density and composition upon nanoparticle (NP) addition. Different columns represent data for proximal, transverse, and distal vessels of the Human Gut Simulator as shown. Nanoparticles were added daily to the base medium after taking samples on day 14 for 7 days. In the control run, silver NPs were used instead of TiO_2. A, the cell density in each vessel. B, calculations of genus level-based community diversity and evenness. C, the cumulative abundances of Gram-positive and Gram-negative bacterial cells. Error bars in panels B and C represent standard deviation of measurements between two replicate runs. D, the cumulative abundance of different bacterial classes at each time point. Abbreviations: NP, nanoparticles.

Table 1. Nanoparticle characterization

Nanoparticles	Hydrodynamic Diameter (nm)		Zeta Potential (mV)	
	Water	Medium	Water	Medium
Titanium dioxide	789.1 ± 282.3[a]	3668.7 ± 668.5[a,b]	−24.5 ± 0.5[c,d]	−10.8 ± 1.3[c,e]
Silver	864.7 ± 201.2	1063.5 ± 521.6[b]	−28.3 ± 0.8[d,f]	−5.6 ± 1.0[e,f]

Data are shown as arithmetic mean ± standard deviation. Lowercase letters denote pairs of values with statistically significant (at $\alpha = .01$) differences based on the two-tail t-test.

the sum of cells of all taxa within each sample equaled the cell density in that sample. Functional capability of microbial communities was predicted using PICRUSt software as we did previously (Agans *et al.*, 2018).

Measurements of short-chain fatty acids. Short-chain fatty acid (SCFA) metabolites were measured in samples from days 14, 21, and 28 of both TiO_2 exposure runs. Collected samples from vessel 1 were centrifuged and then filtered through 0.22 μm syringe nylon filter. Alltech Econoshere C18 5 U column was used to separate SCFAs on the BioRad BioLogic DuoFlow high performance liquid chromatography (HPLC) system. The mobile phase was 50 mM NaH_2PO_4 buffer (pH 2.8) with 1% acetonitrile and was pumped at 1 ml/min. Metabolite concentrations were calculated by comparing sample peaks to standards of each SCFA measured separately at 3, 10 , and 100 mM.

Statistical analyses. Multivariate statistical analyses were carried out on the genus-level microbial abundance dataset following the approaches we described previously (Paliy and Shankar, 2016). Matlab and R-based scripts were used to run all algorithms. Output from PICRUSt was processed through STAMP statistical software (Parks *et al.*, 2014).

RESULTS

Nanoparticle Characterization

Nanoparticles range in size, shape, and charge; characteristics which can be further modified by biological materials. Thus, we first characterized physicochemical properties of TiO_2 and Ag NPs. Nanoparticles were dispersed in both water and HGS medium and checked for hydrodynamic diameter. Both materials exhibited a similar diameter in water, however, when dispersed in HGS medium, TiO_2 displayed a significantly larger diameter compared with Ag NPs (Table 1). Interestingly, the charge of each material was also relatively similar in water but different upon dispersion in HGS medium, with Ag NPs showing greater transition toward neutral charge than TiO_2 NPs. Although TiO_2 and Ag NPs appear to interact differently with HGS medium components, their inherent physical properties were sufficiently similar to enable the use of Ag NPs as control.

Nanoparticle Interactions With Human Microbiota

Human gut microbial communities were established in the HGS system for 14 days. At that time, the microbiota was exposed to TiO_2 NPs (or Ag NPs in the control run) daily for 7 days. Cell densities in each vessel were measured frequently as shown in Figure 1A. Addition of 100 mg/day of TiO_2 NPs to HGS elicited a modest drop (19.5% on average) in community cell density. Such effect was drastically more profound in the control run: addition of silver NPs to the community led to a 62.0% reduction on average in culture density (see Figure 1A). When addition of NPs was ceased, community recovered fully within 1 day for

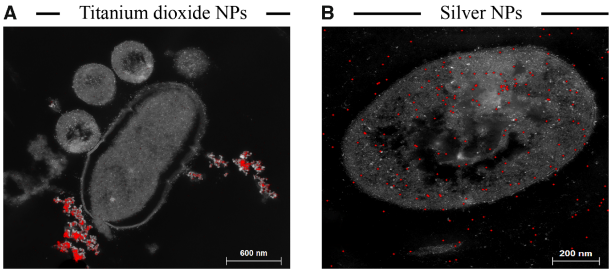

Figure 2. Visualization of the association of TiO_2 and Ag nanoparticles with microbial cells. Cells and medium components are shown in grayscale. Nanoparticles are shown as bright dots. Note different magnification scale of the two images.

TiO_2 NPs runs and within 5 days for the Ag NPs run, thus providing further support that NP addition was the primary cause of community density reduction during preceding week.

In agreement with hydrodynamic diameter measurements, electron spectroscopy revealed that TiO_2 NPs formed large agglomerates that appeared to loosely interact with microbial cells. These TiO_2 agglomerates could be often found in close proximity to cells or immediately against a cell membrane (Figure 2A). Silver NPs were found both within and outside microbial cells (Figure 2B). Silver NPs were of notably smaller size and appeared to not be aggregated. These differences in physical interaction of TiO_2 and Ag NPs might explain, at least in part, the significantly lower effect of TiO_2 NPs on community growth.

TiO_2 NPs Do Not Change Microbial Community Composition

We used 16S rRNA gene sequencing to evaluate microbial community composition changes during TiO_2 NPs addition. Despite changes in overall culture densities, community diversity and evenness remained stable throughout each run (Figure 1B). The overall numbers of Gram-positive and Gram-negative cells fluctuated little during the runs (Figure 1C), and the proportions of microbial classes were also similar across all samples (Figure 1D). All vessels were dominated by two microbial classes of Clostridia and Bacteroidia, with significant numbers of Verrucomicrobia (represented mostly by mucin-degrading genus *Akkermansia*) also appearing in the transverse and especially distal vessel (Agans *et al.*, 2018). To estimate which factors contributed to the observed microbiota structure, we carried out a constrained canonical ordination analysis (CCA) of microbial genus abundances using vessel type, replicate run, and NP addition as three explanatory variables (Paliy and Shankar, 2016). As displayed in Figures 3A and B, samples were distributed in the CCA ordination space based primarily on the vessel type and replicate run. Vessel identity explained more than 69% of the overall microbiota composition variability among samples. In contrast, the presence of TiO_2 NPs in the medium contributed less than 5% to the microbiota structure differences.

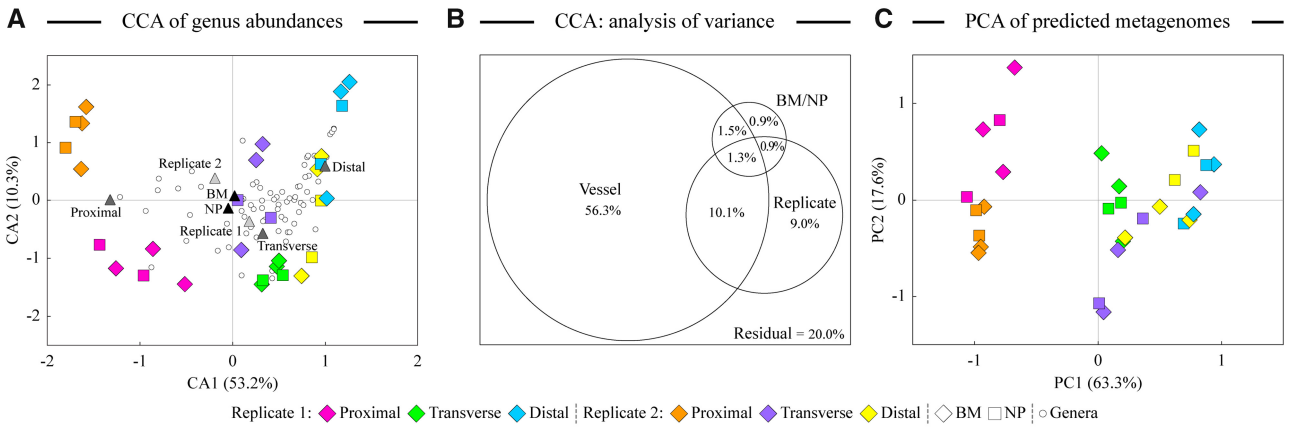

Figure 3. Analysis of community composition and predicted functional capacity. A, the output of the constrained canonical correspondence analysis (CCA). Medium type (base or with NPs), vessel identity, and replicate run were used as explanatory variables that constrained the variability of the genus abundance dataset. The analysis of variance of the CCA output (B) depicts the relative contribution of explanatory variables to the overall variability in the microbial abundance dataset. C, the results of the principal components analysis (PCA) of predicted metagenome-encoded microbial functions. Abbreviations: CCA, canonical correspondence analysis; PCA, principal components analysis.

Microbial Functionality and Fermentation Are Not Altered Upon TiO_2 NP Addition

We used PICRUSt algorithm to predict microbiota functional capacities in each sample based on its community composition. Principal components analysis (PCA) was then used to evaluate the similarities among predicted metagenomes of all profiled samples. As shown in Figure 3C, distribution of samples in PCA space was also associated mostly with the vessel identity and run number. We observed no significant differences between the predicted metagenomes of the communities during the NP challenge period compared with the community establishment or rescue periods. These results are consistent with our observations that NP challenge reduced the culture density but did not affect community members discriminately. We also measured levels of SCFA, end products of microbial fermentation, in the same samples (Table 2). No statistically significant differences were evident for communities subjected to TiO_2 NPs in comparison to the establishment and rescue time points.

Table 2. Concentrations (mM) of short-chain fatty acids in proximal vessel

Short-chain fatty acid	Day 14	Day 21	Day 28
Acetate	100.9 ± 7.8	98.4 ± 16.5	89.2 ± 27.8
Butyrate	121.7 ± 3.1	119.0 ± 3.9	119.1 ± 2.3
Lactate	33.5 ± 2.1	32.4 ± 0.1	35.3 ± 4.0
Propionate	52.6 ± 2.0	48.0 ± 3.4	47.9 ± 1.4

Data are shown as arithmetic mean ± standard deviation. No statistically significant (at $\alpha = .01$) differences were found based on the two-tail t-test.

DISCUSSION

The continued manufacturing and inclusion of ENMs in consumer products make them a persistent factor in human health. Although most of the previous focus on ENMs revolved around acute exposures via respiratory route, much importance has been given recently to ingested NPs due to their potential impact on gut microbiota. Here, we evaluated the impact of TiO_2 nanomaterial on human gut microbiota, and contrasted its effect with that of Ag NPs with well-known bactericidal properties (Vimbela *et al.*, 2017). When added to HGS medium, TiO_2 exhibited strong agglomeration compared with Ag, possibly as a result of titanium being able to interact with broad organic species such as proteins (Loosli *et al.*, 2015). Furthermore, TiO_2 was primarily located outside the cells in close proximity to cell walls (see Figure 2A). We can speculate that the lack of TiO_2 within cells might be attributed to the generation of TiO_2 agglomerates, which prevent active internalization into the cells. The formation of such large agglomerates could also potentially explain the lower toxicity of TiO_2 NPs in comparison with Ag NPs (Lin *et al.* 2014). In contrast, Ag NPs were found within cells and cell debris, most likely owing to their smaller size due to lack of agglomeration.

These differences in NP interactions were associated with the distinct patterns of microbial community response to TiO_2 and Ag NP presence in the medium. Silver drastically reduced community density, whereas TiO_2 only elicited a modest inhibitory effect on microbiota (see Figure 1A). This latter effect seemed to affect different microbial taxa similarly and did not lead to any noticeable changes in community composition (Figures 1 and 3). The TiO_2 effect on the microbial community might thus be indirect and can involve, for example, partial sequestration of environmental components in NP agglomerates, thus lowering nutrient availability in the environment (Luby *et al.*, 2016). Alternatively, association of TiO_2 agglomerates with cell membranes might inhibit the cell's ability to divide or interfere with the absorption of nutrients from the environment.

Potential limitations of this study included (1) the use of *in vitro* HGS system that did not contain host tissues and metabolites; (2) the assessment of microbiota functional capacities was based on metagenome predictions, and (3) we only focused on SCFAs in our metabolite analyses. Thus, our findings do not rule out potential alterations in the human gut as a result of the exposure of host tissues to TiO_2 NPs, and it is also possible that there might be other functional and metabolic changes in the microbial communities that we have not detected.

DECLARATION OF CONFLICTING INTERESTS

The authors declared no potential conflicts of interest with respect to the research, authorship, and publication of this article.

FUNDING

This work was supported by the Dayton Area Graduate Studies Institute award RH15-WSU-15-1 to RA, AG, and OP, and by the National Science Foundation award DBI-1335772 to OP.

REFERENCES

Agans, R., Gordon, A., Kramer, D. L., Perez-Burillo, S., RufiÃ¡n-Henares, J. A., and Paliy, O. (2018). Dietary fatty acids sustain the growth of the human gut microbiota. *Appl. Environ. Microbiol.* **84**, e01525-18.

Bakand, S., Hayes, A., and Dechsakulthorn, F. (2012). Nanoparticles: A review of particle toxicology following inhalation exposure. *Inhal. Toxicol.* **24**, 125–135.

Basinas, I., Jiménez, A. S., Galea, K. S., Tongeren, M. v., and Hurley, F. (2018). A systematic review of the routes and forms of exposure to engineered nanomaterials. *Ann. Work Exposures Health* **62**, 639–662.

Caporaso, J. G., Kuczynski, J., Stombaugh, J., Bittinger, K., Bushman, F. D., Costello, E. K., Fierer, N., Pena, A. G., Goodrich, J. K., Gordon, J. I., *et al.* (2010). QIIME allows analysis of high-throughput community sequencing data. *Nat. Methods* **7**, 335–336.

Gorkiewicz, G., and Moschen, A. (2018). Gut microbiome: A new player in gastrointestinal disease. *Virchows Arch.* **472**, 159–172.

Gunawan, C., Lim, M., Marquis, C. P., and Amal, R. (2014). Nanoparticle–protein corona complexes govern the biological fates and functions of nanoparticles. *J. Mater. Chem. B* **2**, 2060–2083.

Hollister, E. B., Gao, C., and Versalovic, J. (2014). Compositional and functional features of the gastrointestinal microbiome and their effects on human health. *Gastroenterology* **146**, 1449–1458.

Hu, X., Li, D., Gao, Y., Mu, L., and Zhou, Q. (2016). Knowledge gaps between nanotoxicological research and nanomaterial safety. *Environ. Int.* **94**, 8–23.

Lin, X., Li, J., Ma, S., Liu, G., Yang, K., Tong, M., and Lin, D. (2014). Toxicity of TiO2 nanoparticles to *Escherichia coli*: Effects of particle size, crystal phase and water chemistry. *PLoS One* **9**, e110247.

Loosli, F., Vitorazi, L., Berret, J. F., and Stoll, S. (2015). Towards a better understanding on agglomeration mechanisms and thermodynamic properties of TiO(2) nanoparticles interacting with natural organic matter. *Water Res.* **80**, 139–148.

Luby, A. O., Breitner, E. K., and Comfort, K. K. (2016). Preliminary protein corona formation stabilizes gold nanoparticles and improves deposition efficiency. *Appl. Nanosci.* **6**, 827–836.

Paliy, O., and Foy, B. D. (2011). Mathematical modeling of 16S ribosomal DNA amplification reveals optimal conditions for the interrogation of complex microbial communities with phylogenetic microarrays. *Bioinformatics* **27**, 2134–2140.

Paliy, O., and Shankar, V. (2016). Application of multivariate statistical techniques in microbial ecology. *Mol. Ecol.* **25**, 1032–1057.

Parks, D. H., Tyson, G. W., Hugenholtz, P., and Beiko, R. G. (2014). STAMP: Statistical analysis of taxonomic and functional profiles. *Bioinformatics* **30**, 3123–3124.

Pietroiusti, A., Bergamaschi, E., Campagna, M., Campagnolo, L., De Palma, G., Iavicoli, S., Leso, V., Magrini, A., Miragoli, M., Pedata, P., *et al.* (2017). The unrecognized occupational relevance of the interaction between engineered nanomaterials and the gastro-intestinal tract: A consensus paper from a multidisciplinary working group. *Part. Fibre Toxicol.* **14**, 47.

Rigsbee, L., Agans, R., Foy, B. D., and Paliy, O. (2011). Optimizing the analysis of human intestinal microbiota with phylogenetic microarray. *FEMS Microbiol. Ecol.* **75**, 332–342.

Sekirov, I., Russell, S. L., Antunes, L. C., and Finlay, B. B. (2010). Gut microbiota in health and disease. *Physiol. Rev.* **90**, 859–904.

van den Brule, S., Ambroise, J., Lecloux, H., Levard, C., Soulas, R., De Temmerman, P. J., Palmai-Pallag, M., Marbaix, E., and Lison, D. (2016). Dietary silver nanoparticles can disturb the gut microbiota in mice. *Part. Fibre Toxicol.* **13**, 38.

Vimbela, G. V., Ngo, S. M., Fraze, C., Yang, L., and Stout, D. A. (2017). Antibacterial properties and toxicity from metallic nanomaterials. *Int. J. Nanomed.* **12**, 3941–3965.

Weir, A., Westerhoff, P., Fabricius, L., Hristovski, K., and von Goetz, N. (2013). Titanium dioxide nanoparticles in food and personal care products. *Environ. Sci. Technol.* **46**, 2242–2250.

West, A. L., Schaeublin, N. M., Griep, M. H., Maurer-Gardner, E. I., Cole, D. P., Fakner, A. M., Hussain, S. M., and Karna, S. P. (2016). In situ synthesis of fluorescent gold nanoclusters by nontumorigenic microglial cells. *ACS Appl. Mater. Interfaces* **8**, 21221–21227.

Wiesenthal, A., Hunter, L., Wang, S., Wickliffe, J., and Wilkerson, M. (2011). Nanoparticles: Small and mighty. *Int. J. Dermatol.* **50**, 247–254.